Genetic alteration of endothelial heparan sulfate selectively inhibits tumor angiogenesis

Mark M. Fuster,[1] Lianchun Wang,[2] Janice Castagnola,[2] Lyudmila Sikora,[4] Krisanavane Reddi,[1] Phillip H.A. Lee,[3,5] Katherine A. Radek,[3,5] Manuela Schuksz,[2] Joseph R. Bishop,[2] Richard L. Gallo,[3,5] P. Sriramarao,[4] and Jeffrey D. Esko[2]

[1]Department of Medicine, Division of Pulmonary and Critical Care Medicine, [2]Department of Cellular and Molecular Medicine, and [3]Division of Dermatology, University of California, San Diego, La Jolla, CA 92093
[4]Division of Vascular Biology, La Jolla Institute for Molecular Medicine, San Diego, CA 92121
[5]Veterans Affairs Medical Center, San Diego, CA 92161

To examine the role of endothelial heparan sulfate during angiogenesis, we generated mice bearing an endothelial-targeted deletion in the biosynthetic enzyme *N*-acetylglucosamine *N*-deacetylase/*N*-sulfotransferase 1 (Ndst1). Physiological angiogenesis during cutaneous wound repair was unaffected, as was growth and reproductive capacity of the mice. In contrast, pathological angiogenesis in experimental tumors was altered, resulting in smaller tumors and reduced microvascular density and branching. To simulate the angiogenic environment of the tumor, endothelial cells were isolated and propagated in vitro with proangiogenic growth factors. Binding of FGF-2 and $VEGF_{164}$ to cells and to purified heparan sulfate was dramatically reduced. Mutant endothelial cells also exhibited altered sprouting responses to FGF-2 and $VEGF_{164}$, reduced Erk phosphorylation, and an increase in apoptosis in branching assays. Corresponding changes in growth factor binding to tumor endothelium and apoptosis were also observed in vivo. These findings demonstrate a cell-autonomous effect of heparan sulfate on endothelial cell growth in the context of tumor angiogenesis.

Introduction

Solid tumors and their metastases require the process of angiogenesis to invest themselves with host microvasculature and to undergo pathologic progression (Folkman, 1992). Blockade of this process leads to tumor arrest and apoptosis (Holmgren et al., 1995). Effective agents include proteolytic fragments of collagen XVIII (endostatin), platelet factor 4 (anginex), TNP-470 (a fumagillin derivative), antibodies against integrins and proangiogenic growth factors (e.g., anti-VEGF antibodies), small-molecule inhibitors of endothelial growth-factor receptors (e.g., VEGF, FGF, and PDGF receptor tyrosine kinase inhibitors), and matrix metalloproteinase inhibitors (Folkman, 1992; Carmeliet and Jain, 2000; Liekens et al., 2001; Ellis, 2005). Many proangiogenic growth factors, in particular, FGF-2 and heparin-binding splice isoforms of VEGF-A, such as $VEGF_{164}$, bind to heparan sulfate proteoglycans expressed on tumor endothelia or in the extracellular matrix, which facilitates formation of signaling complexes composed of the ligands and their receptor tyrosine kinases (Iozzo and San Antonio, 2001; Jiang and Couchman, 2003; Presta et al., 2005). The dependence of receptor activation on heparan sulfate suggests that endothelial heparan sulfate might represent a therapeutic target and that inhibitors might have synergistic effects because of interference with multiple growth factor signaling pathways important for tumorigenesis.

Binding of both FGF-2 and $VEGF_{164}$ depends on the sulfation state of heparan sulfate, in particular *N*-sulfation of glucosamine residues in specific domains along the heparan sulfate chain (Yayon et al., 1991; Turnbull et al., 1992; Ono et al., 1999). A family of four *N*-acetylglucosamine *N*-deacetylase/*N*-sulfotransferases (Ndst) catalyze this reaction (Esko and Selleck, 2002), but microvascular endothelial cells only express *Ndst1* and *Ndst2* (Wang et al., 2005). *Ndst2*-deficient mice are essentially normal, aside from defective granule formation in connective tissue-type mast cells (Forsberg et al., 1999; Humphries et al., 1999). In contrast, mice with a systemic deletion of *Ndst1* die perinatally because of forebrain defects, skeletal malformation, and lung hypoplasia (Ringvall et al., 2000; Grobe et al., 2005; Pan et al., 2006; Pallerla et al., 2007), but vasculogenesis and angiogenesis up to birth appear normal by gross examination and general histology. Here, we show that altering Ndst1 expression in endothelial cells alters growth of syngeneic murine tumors because of a unique alteration in the

Correspondence to Jeffrey D. Esko: jesko@ucsd.edu

Abbreviations used in this paper: LLC, Lewis lung carcinoma; Ndst, *N*-deacetylase/*N*-sulfotransferase.

The Journal of Cell Biology, Vol. 177, No. 3, May 7, 2007 539–549
http://www.jcb.org/cgi/doi/10.1083/jcb.200610086

tumor microvasculature. In contrast, the mutation had no effect on physiological angiogenesis, e.g., during cutaneous wound repair. The change in tumor angiogenesis appears to result from altered binding and signaling by the proangiogenic growth factors FGF-2 and VEGF.

Results

Physiological angiogenesis is unaffected by altering Ndst1 expression in endothelial cells

To determine the role of Ndst1 in angiogenesis in adult animals, mice harboring a conditional loxP-flanked allele of *Ndst1* (*Ndst1*$^{f/f}$) were crossed with transgenic mice expressing the bacteriophage recombinase Cre under the control of the angiopoietin receptor (*Tek*) promoter, which is expressed in a pan-endothelial fashion (Constien et al., 2001; Kisanuki et al., 2001). *Ndst1*$^{f/f}$*TekCre*$^{+}$ (mutant) and *Ndst1*$^{f/f}$*Tek*Cre^{-} (wild type) mice were recovered at the expected Mendelian frequency and showed the normal pattern of weight gain, indicating that vasculogenesis and physiological angiogenesis were sufficient for normal development. Adult mutant mice were indistinguishable from their wild-type littermates in general health, behavior, and body weight (Wang et al., 2005). *Ndst1*$^{f/f}$*TekCre*$^{+}$ females also reproduced normally and had normal litter sizes, indicating that sufficient reproductive angiogenesis occurred to allow for normal colony propagation.

Physiological angiogenesis during cutaneous wound repair also appeared normal. After a biopsy punch wound of dorsal skin, an intense angiogenic response was detected 3–4 d after injury at the granulating edges of healing wounds. Both mutant and wild-type mice showed a similar response in clustering of CD31-positive processes at the wound margin (Fig. 1 a). No significant difference in the density of processes at the wound edges was noted between the two groups (Fig. 1 b). Vascular density fell with distance from the wound margin in a similar fashion in both mutant and wild-type mice as well. The rate of wound contraction over the 4-d period also did not differ (Fig. 1 c), and in separate experiments, complete resolution of wounds occurred in both groups of mice by 10 d. Analysis of retinal vascular development under normoxic conditions showed only a very minor effect that was not significant (Friedlander, M., personal communication). These findings suggest that physiological angiogenesis was unaffected by endothelial inactivation of *Ndst1*.

Tumor growth is reduced in *Ndst1*$^{f/f}$*TekCre*$^{+}$ mice

To study the effect of inactivation of *Ndst1* on pathological angiogenesis, syngeneic Lewis lung carcinoma (LLC) cells were injected subcutaneously in the hindquarters of *Ndst1*$^{f/f}$*TekCre*$^{+}$ and *Ndst1*$^{f/f}$*Tek*Cre^{-} mice. As shown in Fig. 2 a, growth of subcutaneous tumors in mutant animals was significantly attenuated ($P < 0.001$) relative to that observed in wild-type littermates at 10 and 15 d after injection. This effect was also seen in a second transplant model in which syngeneic mouse melanoma (B16BL6) tumors were injected subcutaneously. Like LLC tumors, melanoma exhibited a marked reduction in mean tumor

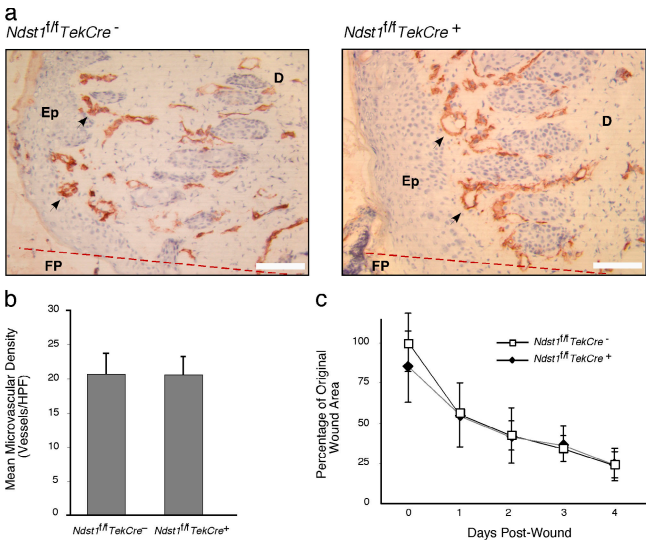

Figure 1. **Wound healing and angiogenesis is not affected in Ndst1-deficient mice.** Mice were subjected to a 3-mm-diameter full-thickness punch lesion on the dorsal skin area. (a) After 4 d, biopsies were taken for immunohistology with CD31 mAb to detect blood vessels in the wound region (arrows). Wounds in both wild-type and mutant mice underwent substantial angiogenesis, as noted by the high density of CD31+ processes detected along the dermis. (b) Density of microvasculature at punch-biopsy wound border, as measured by mean number of CD31+ microvessels per 400× microscopic field surrounding the wound center, is shown for each genotype (mean density calculated from four fields taken about wound center for each mouse; $n = 8$ mice per group). No significant difference was noted between mutant and wild-type mice ($P = 0.96$). (c) Contraction of the wound area during healing was measured daily. No significant differences were observed between mutant and wild-type mice ($P = 0.288$). Anatomic structures in panel a include the wound fibrin plug (FP), located to one side of the original wound margin (represented by the dotted red line), bordered by a proliferating epithelial (Ep) layer and dermis (D). Error bars indicate SD. Bars, 50 μm.

volume in mutant mice compared with wild-type littermates at 10 d (52% reduction in mean volume; $P < 0.02$). Because skin ulceration occurred and the animals showed signs of morbidity after 15 d, all tumor growth experiments were terminated as required by Association for Assessment and Accreditation of Laboratory Animal Care (AAALAC) guidelines for the humane treatment of animals.

Because the *TekCre* transgene is expressed in endothelial cells, leukocytes, and marrow-derived endothelial precursors (Constien et al., 2001; Kisanuki et al., 2001), we performed bone marrow transplantation experiments to determine the relative contributions of these cell populations to the phenotype. Mutant mice transplanted with wild-type marrow showed persistent attenuation in tumor growth, indicating that deletion of *Ndst1* in tissue-resident endothelia was sufficient to achieve a marked alteration in tumor growth (Fig. 2, compare a and b, center). Transplantation of wild-type mice with mutant marrow did not alter tumor growth (Fig. 2 b, right), indicating that alteration of heparan sulfate in marrow-derived cells had no effect. Control transplantations in which the genotype of the marrow donor and the recipient mouse were matched showed the expected results (Fig. 2 b, left). These experiments exclude factors such as altered tumor immunity because of changes in leukocyte heparan sulfate. Histological examination of the tumors

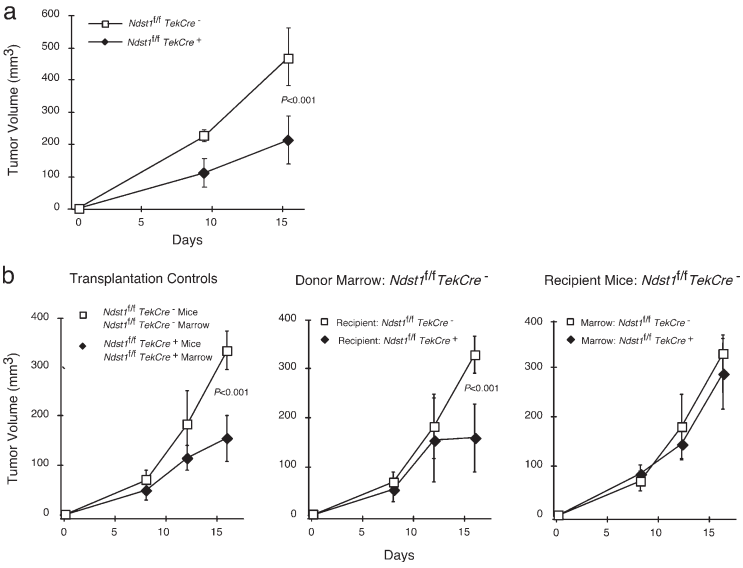

Figure 2. **Tumor growth is reduced in *Ndst1*$^{f/f}$*TekCre*$^{+}$ mutant mice.** (a) LLC (4×10^5 cells) were injected into the hindquarters of either *Ndst1*$^{f/f}$*TekCre*$^{+}$ or *Ndst1*$^{f/f}$*TekCre*$^{-}$ mice ($n = 5$ per group). Tumor volume was estimated by caliper measurements at the indicated times. (b) To control for the genotype of hematopoietic tissue among the various mice, mutant ($n = 5$) and wild-type ($n = 7$) mice were transplanted with bone marrow from genotype-matched mice (b, left). A separate group of mutant mice ($n = 5$) was transplanted with wild-type marrow (b, middle), and a group of wild-type mice was transplanted with mutant bone marrow (b, right). Tumor growth consistently tracked with the genotype of the recipient mouse, indicating that differences in heparan sulfate in the host endothelium were responsible for the altered growth of the tumors. Error bars indicate SD.

also showed that tumor infiltration by CD45/Gr-1–positive granulocytes was not statistically different in the mutant, suggesting that reduced acute leukocyte infiltration caused by altered endothelial heparan sulfate (Wang et al., 2005) did not affect tumor growth. These findings also exclude effects due to marrow-derived endothelial precursors, which can serve as early contributors to vascularization in some tumors (Lyden et al., 2001; Shinde Patil et al., 2005).

Tumor microvasculature in mutant mice is altered

To determine whether the decrease in tumor mass was caused by a change in tumor microvasculature, we examined the pattern of staining of CD31 (PECAM-1 [platelet/endothelial cell adhesion molecule-1]) in tumor sections (Fig. 3). Microvascular density was significantly reduced in tumors grown on the mutant background (Fig. 3 b; 26.8 ± 4.7 vs. 35.3 ± 4.7 microvessels per 400× field in mutant and wild-type mice, respectively; $P < 0.02$). A slight increase in vessel caliber was also apparent when antibody binding was visualized by fluorescence microscopy (Fig. 3 b).

To obtain greater morphometric detail, intravital microscopy was used to assess microvascular branching, density, skeletal length, and caliber in LLC tumor spheroid preparations implanted on dorsal skinfold chambers. Views of tumor microvasculature at 12 d after implantation revealed a general reduction in vascular density and complexity within tumors grown in the mutant (Fig. 3 c). Morphometric analysis of digitized images showed a marked reduction in degree of branching, density of linearized vasculature (grid intersection), and skeletal length (Fig. 3, d and e). A small, but statistically significant ($P < 0.02$) increase in vascular caliber was noted as well. These alterations may have resulted from a primary branching defect of tumor neovasculature (Parsons-Wingerter et al., 2000) and are similar to changes in vascular development after in vivo treatment with anti-VEGF antibodies or VEGF receptor tyrosine kinase inhibitors (Yuan et al., 1996; Jain, 2003) and alterations in FGF-dependent bud formation and branching morphogenesis of respiratory epithelium during *Drosophila melanogaster* tracheal development (Lin et al., 1999) and vertebrate lung development (Izvolsky et al., 2003).

Altered binding of FGF-2 and VEGF$_{164}$ to endothelial heparan sulfate

To gain insight into the mechanism underlying the alteration in tumor vascularization, we attempted to purify endothelial cells from tumors and normal tissues. However, we were unable to obtain sufficient numbers of cells from tumors, and the cultures were overtaken rapidly by small numbers of contaminating tumor cells. In contrast, highly purified cells were obtained from lungs and livers of mutant and wild-type mice. These cells proliferated for two to three passages in culture, and each population maintained their differentiated phenotype based on CD31 expression (Fig. 4 a), positive staining for von Willebrand Factor, and uptake of DiI-labeled acetylated low-density lipoprotein (Wang et al., 2005). Both mutant and wild-type endothelial cells grew at comparable rates in culture (in medium supplemented with heparin, endothelial cell growth supplement, and 20% FBS; Fig. 4 b). Omission of heparin from the growth medium mildly decreased growth of both mutant and wild-type cells. Thus, isolated cells showed no obvious effect of Ndst1 deficiency on proliferation in monolayer culture.

The extent of deletion of the *Ndst1*$^{f/f}$ allele in endothelial cells from *TekCre*$^{+}$ mice was >95%, as measured by quantitative PCR, consistent with values obtained by Southern blotting (Wang et al., 2005). Examination of expression of *Ndst1-4* expression by quantitative RT-PCR showed >95% reduction in *Ndst-1* message in mutant cells, without any significant change in expression of *Ndst2-4* (unpublished data). Analysis of disaccharides liberated from heparan sulfate by heparinase degradation showed a reduction of *N*-sulfated units, leading to an overall 2.3-fold reduction in glucosamine *N*-sulfate (Fig. 4 c). Residual *N*-sulfation presumably arose from the action of *Ndst2* (Ledin et al., 2006). Because of the dependence of downstream *O*-sulfotransferases on *N*-sulfation (Esko and Selleck, 2002), the degree of glucosamine 6-*O*-sulfation and uronyl-2-*O*-sulfation of

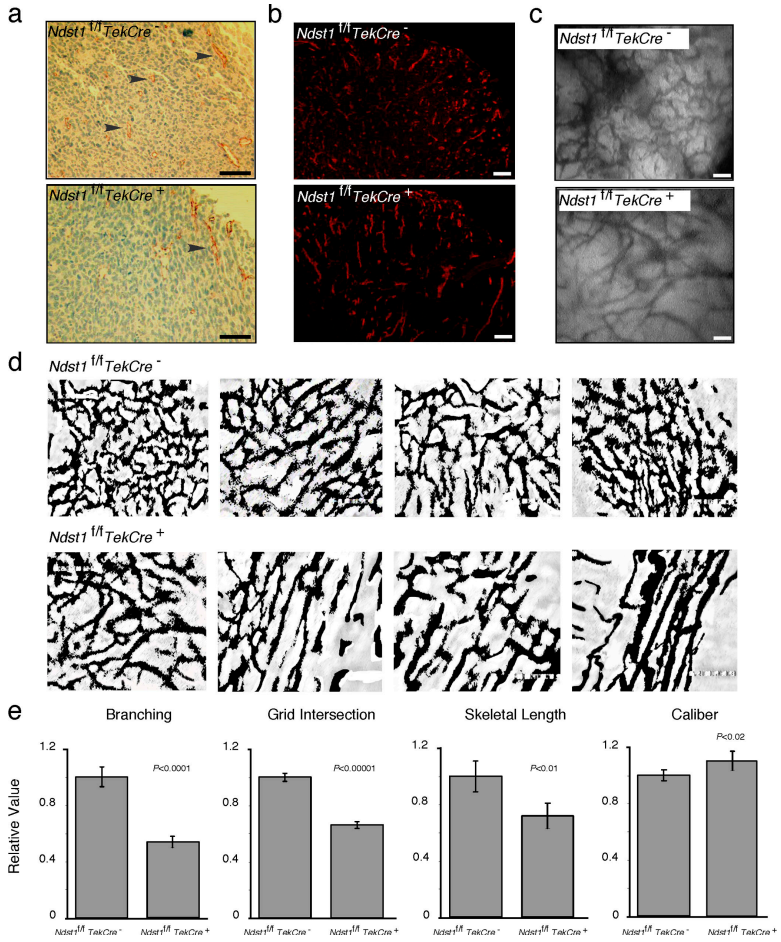

Figure 3. **Visualization of altered tumor microvasculature in *Ndst1*$^{f/f}$*TekCre*$^{+}$ mice.** (a) After 15 d, tumor sections were prepared and stained with CD31 mAb (examples of vessels are indicated by black arrowheads). (b) Vessels were stained with anti-CD31 mAb and visualized by fluorescence microscopy as well. (c) Intravital videomicroscopy of tumor vascular morphology. Representative photomicrographs of tumor spheroid microvasculature 12 d after implantation into skinfold chambers are shown for wild-type (top) and mutant (bottom) spheroids. (d) Representative digitized images of spheroid microvasculature from four independent mice. The first image in each set corresponds to the photomicrographs shown in panel c. (e) Digitized images of four to six regions per chamber were recorded at 100× magnification and scanned and quantified for microvascular branching, grid intersection, linear skeletal length, and caliber. Error bars indicate SD. Bars, 100 μm.

chains was reduced as well (Fig. 4 c). The change in heparan sulfate structure led to a decrease in cell-surface binding of FGF-2 and $VEGF_{164}$ to mutant endothelia compared with cells derived from wild-type animals (Fig. 4 d). In contrast, binding of EGF, which does not require heparan sulfate, was unaffected by the mutation. Binding of FGF-2 and $VEGF_{164}$ to ^{35}S-radiolabeled heparan sulfate isolated from the mutant endothelia was reduced as well (Fig. 4 e).

Altered signaling responses of mutant endothelial cells to FGF-2 and $VEGF_{164}$

Under standard culture conditions, wild-type and mutant primary endothelia proliferated at similar rates and to the same extent (Fig. 4 b), but striking differential growth responses of cells were observed when cells were cultivated on Matrigel and supplemented with FGF-2 or $VEGF_{164}$. Wild-type endothelia proliferated and formed extensive branched networks in response to 1–10 ng/ml FGF-2, whereas mutant cells were unresponsive (Fig. 5, a and b). Increasing the concentration of FGF-2 to values in excess of the physiological range (100 ng/ml) was sufficient to stimulate a sprouting response by mutant cells (Fig. 5 b, right), indicating that they expressed functional FGF receptors that were not activated at lower doses of FGF-2. Treating wild-type cells with heparinase, which degrades heparan sulfate, mimicked the phenotype of the mutant (Fig. 5 c). The addition of unfractionated heparin also blocked the response, whereas it had no effect on mutant cells (even at low concentration). Mutant cells also failed to respond to $VEGF_{164}$, whereas wild-type cells sprouted robustly in response to this factor (Fig. 5 d). Infecting endothelial cells derived from *Ndst1*$^{f/f}$*Tek*Cre^{-} mice with Adenoviral-Cre yielded comparable results (unpublished data), indicating that the effect was cell autonomous and not the result of selection of unresponsive cells during their cultivation.

When mutant cells failed to sprout on Matrigel, the cells remained predominantly clustered and harbored frequent apoptotic cells (Fig. 6 a), consistent with the idea that the alteration in heparan sulfate led to decreased growth responses through the relevant receptor tyrosine kinases (FGFR1, FGFR2, and VEGFR2). Western blotting studies with antibodies showed no change in receptor expression (unpublished data). Addition of FGF-2 to wild-type endothelia resulted in marked phosphorylation of Erk1/2 after 10 min of stimulation, and the signal was sustained for 60 min (Fig. 6 b, top). Mutant endothelial cells, however, exhibited about a threefold reduction in signaling at both time points. VEGF-dependent Erk1/2 phosphorylation was even more dramatically affected. Wild-type cells responded robustly by 10 min, and the signal declined by 60 min. In contrast, mutant cells were essentially unresponsive to VEGF (Fig. 6 b, bottom). Treatment of wild-type cells with heparinase caused similar effects (unpublished data). FGF-2 and VEGF had only a modest effect of phosphorylation of PKB/Akt in either wild-type or mutant cells (Fig. 6 c).

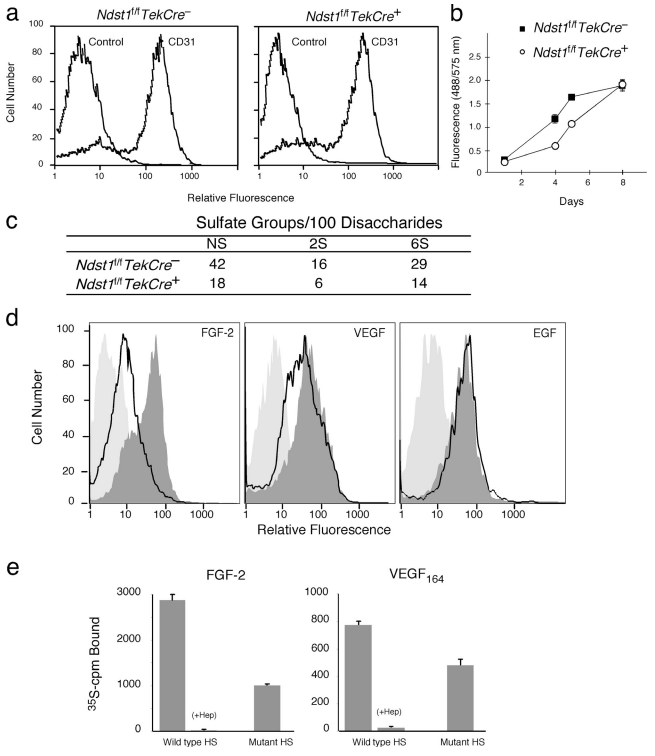

Figure 4. **Binding of FGF-2 and $VEGF_{164}$ to *Ndst1* mutant microvascular endothelia is reduced.** Primary lung microvascular endothelia were isolated from *Ndst1*$^{f/f}$*TekCre*$^{+}$ or *Ndst1*$^{f/f}$*TekCre*$^{-}$ mice (Materials and methods). (a) Flow cytometry of cells with CD31 mAb showed a high degree of purity. Control incubations contained isotype-matched IgG as primary antibody. (b) Proliferation of mutant versus wild-type primary endothelia in cell culture. Fluorescence in the assay is directly proportional to number of viable cells. Measurements for each time point were performed in triplicate, and the values represent the mean ± SD. (c) The extent of glucosamine *N*-sulfation, uronyl 2-*O*-sulfation, or glucosamine 6-*O*-sulfation was determined by disaccharide analysis of heparan sulfate isolated from mutant and wild-type endothelial cells. (d) Binding of biotinylated FGF-2, $VEGF_{165}$, and EGF to isolated wild-type (dark gray profiles) and mutant (unfilled black curve) endothelial cells. Controls consisted of cells treated only with streptavidin-FITC (light gray profiles). (e) Equal amounts of growth factor were added to purified heparan [^{35}S]sulfate isolated from mutant and wild-type endothelial cells, and complexes were collected by membrane filtration. Binding of growth factor in the presence of heparin (+Hep) is shown as a control. Error bars indicate SD.

Decreased growth factor binding to tumor endothelium in vivo

To determine whether the altered responses of endothelial cells in vitro corresponded to changes in growth factor binding in vivo, the distribution of FGF-2 and VEGF was measured in tumor sections. Immunohistochemical analysis of endogenous FGF-2 in tumors showed diffuse staining throughout the tissue regardless of genotype (unpublished data). Incubation of samples with biotinylated FGF-2 also showed a diffuse distribution of binding sites throughout the tumor stroma. However, close inspection of the vasculature revealed intense staining in the perivascular zones in tumors from wild-type mice, a region rich in basement membrane–type heparan sulfate proteoglycans (Fig. 7 a, solid arrowheads; Iozzo, 2005). In contrast, tumors from mutant animals showed a marked reduction in staining (Fig. 7 a, open arrowheads), consistent with decreased binding to endothelial cell–derived heparan sulfate (Fig. 4, d and e).

In contrast to endogenous FGF-2, we were able to examine the localization of endogenous VEGF in the tumor microvasculature using GV39M mAb, which binds to complexes between VEGF-A and its major signaling receptor VEGFR-2/flk-1 (Brekken et al., 1998; Joyce et al., 2005). Immunofluorescence of tumor sections from wild-type mice demonstrated a subset of vessels that stained strongly (Fig. 7 b, top). Many of these vessels also stained for laminin, consistent with studies that showed VEGF in association with basement membranes in some vascular beds (Brekken, R., personal communication). Vessel-associated GV39M was localized in a predominantly abluminal orientation relative to CD31 (Fig. 7 c), supporting the idea that endothelial VEGFR-2 engages VEGF from the stromal side of the vessel (Qu-Hong et al., 1995; Brekken and Thorpe, 2001). Mutant tumor sections stained less strongly with GV39M mAb, especially in laminin-associated vessels (Fig. 7 b, bottom). Interestingly, the distribution of laminin, which also binds heparan sulfate, was not grossly affected. Pericyte investment, as detected by mAb against smooth muscle cell actin, also was not significantly affected by the mutation (Fig. 7 d). Combined CD31/TUNEL staining of tumor sections from mutant mice revealed several apoptotic nuclei associated with walls of the microvasculature that were not present in wild-type tumors (Fig. 7 e), consistent with the in vitro data presented in Fig. 6.

Because the Ndst1 deficiency affected vessel-associated VEGF–VEGFR-2 complexes (Fig. 7 b), we examined whether tumor growth depended on VEGFR-2 expression. When LLC tumors were grown in VEGFR-2 heterozygous mice, mean tumor volumes were reduced by ∼50% compared with the wild type ($P < 0.0001$; Fig. 7 f). CD31-stained tumor sections from VEGFR-2 mutants also exhibited reduced microvascular density (33% reduction relative to wild type; $P < 0.03$) and increased vessel caliber (Fig. 7 g) similar to that described for tumors grown in *Ndst1*$^{f/f}$*TekCre*$^{+}$ mice (Fig. 3).

Discussion

We have demonstrated that altering Ndst1 expression in endothelial cells results in decreased tumor angiogenesis and tumor growth. Vascular changes in the tumor included decreased vessel density and branching and increased caliber of the remaining vessels. These changes correlated with diminished endothelial process formation in vitro in response to FGF-2 and $VEGF_{165}$, altered growth factor binding to isolated endothelial cells and heparan sulfate, and attenuation of Erk1/2 signaling. Altering endothelial heparan sulfate decreased the association of FGF-2 and VEGF with the tumor vasculature in vivo and increased endothelial apoptosis in both branching assays as well as the tumor vasculature. These findings correlate changes in endothelial cell growth mediated by FGF-2 and VEGF to decreased vascularization of the tumor, which in turn diminished tumor growth.

Recently, Jakobsson et al. (2006) showed that VEGF signaling in endothelial cells and angiogenesis were fully supported by heparan sulfate expressed in trans by adjacent perivascular smooth muscle cells. Given the selective deletion of Ndst1 in endothelial cells in *Ndst1*$^{f/f}$*TekCre*$^{+}$ mice and the fact that pericyte density was unaltered (Fig. 7 d), it would appear that pericyte

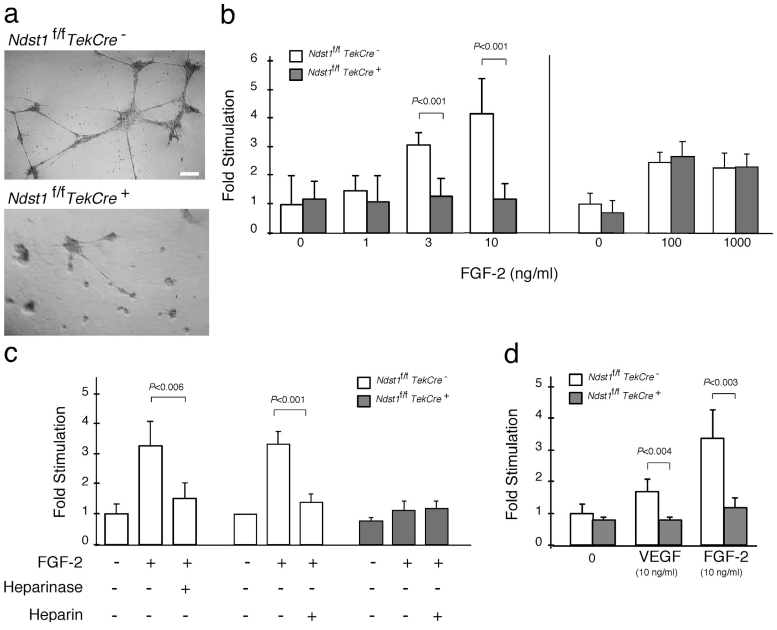

Figure 5. **Altered sprouting of Ndst1-deficient microvascular endothelial cells on reconstituted extracellular matrix.** (a) Wild-type endothelial cells formed extensive networks of interconnected processes when plated on Matrigel with FGF-2 at 10 ng/ml (top). Under the same conditions, sprouting of mutant cells was markedly impaired (bottom). Bar, 200 μm. (b) Process formation by wild-type cells varied with concentration of FGF-2, whereas mutant cells showed essentially no sprouting under these conditions. Treatment with saturating levels of growth factor (100 ng/ml) was sufficient to restore sprouting by mutant cells. (c) Sprouting by wild-type cells to 10 ng/ml FGF-2 was inhibited by the addition of either 3 mU/ml heparinase or 100 μg/ml heparin, whereas the marginal sprouting by mutant cells was unaffected. Data are mean values ± SD for net length of endothelial processes per (100×) microscopic field, normalized to the response of unstimulated wild-type cells. (d) Mutant cells were also insensitive to 10 ng/ml $VEGF_{164}$. Data are the mean ± SD of three independent experiments normalized to the response of unstimulated wild-type endothelia.

heparan sulfate will not substitute for endothelial heparan sulfate during tumor angiogenesis. Thus, in the context of tumor vasculature, endothelial heparan sulfate behaves in a cell-autonomous manner. Ideally one would like to further potentiate the phenotype by more dramatic changes in heparan sulfate composition or content. However, complete ablation of sulfation (*Ndst1*$^{-/-}$*Ndst2*$^{-/-}$) or inhibition of the polymerase that catalyzes formation of the heparan sulfate chains (*Ext1/Ext2*) result in early developmental defects, including failure to differentiate mesodermal precursors of the endothelium (Lin et al., 2000; Holmborn et al., 2004; Stickens et al., 2005), thus preventing further studies of the vasculature in adult animals.

Vasculogenesis (endothelial cell differentiation/de novo vessel formation) and physiological angiogenesis appear to be unaffected in *Ndst1*$^{f/f}$*TekCre*$^{+}$ mice based on normal birth weight, growth of the animals, reproductive capacity, and normal cutaneous wound healing (Fig. 1). Nevertheless, endothelial cells derived from the lungs of mutant animals showed alterations in growth factor binding, signaling, and sprouting behavior under conditions that promote proliferation in vitro (Figs. 4–6). Why, then, was angiogenesis selectively altered in the tumor environment but not under conditions of cutaneous wound repair? One possibility is that the tumor microenvironment places an especially high demand on the tumor vascular bed with respect to transfer of nutrients, removal of waste products, and gas exchange. If correct, then further stress, e.g., by hypoxia or induced tissue regeneration, might reveal underlying differences in angiogenic capacity in normal tissues. Alternatively, the composition of growth factors might differ in the wound environment, or other glycosaminoglycans, such as dermatan sulfate, which is abundant in wound tissue, might compensate for reduced heparan sulfate in the endothelium (Penc et al., 1998; Taylor et al., 2005). Further studies are needed to address this point.

As observed in other tumor models, the microvasculature in LLC tumors displayed a highly chaotic morphology compared with normal vasculature (Carmeliet and Jain, 2000; Jain, 2005). Altering heparan sulfate specifically in the endothelium resulted in less branched and tortuous tumor vessels and decreased overall density of the neovasculature (Fig. 3). Similar morphological changes have been observed in tumor microvasculature after in vivo treatment with anti-VEGF antibodies or VEGF receptor tyrosine kinase inhibitors (Yuan et al., 1996; Jain, 2003), suggesting that altering heparan sulfate in the endothelium may preferentially affect VEGF-mediated responses. Other observations that support this idea include the following: (1) transfection of VEGF nullizygous tumor cells with $VEGF_{164}$ rescues tumor growth and vascular density/branching, whereas altered tumor growth and a hypobranched/hypodense vasculature results from transfection with the non–heparin binding isoform, $VEGF_{120}$ (Grunstein et al., 2000); (2) mouse embryos engineered to express only $VEGF_{120}$ exhibit a marked decrease in capillary branching accompanied by increased vascular caliber (Ruhrberg, 2003); (3) altering Ndst1 expression reduces the formation of VEGF–VEGFR complexes in mutant tumor vasculature (Fig. 7 b); and (4) reduction of expression of *VEGFR2* in heterozygous mutants resulted in reduced tumor growth and vascularization (Fig. 7, f and g). The modest dilatation of mutant tumor microvasculature that we observed could reflect incomplete inactivation of VEGF signaling, as the deficiency in Ndst1, although nearly fully penetrant, does not completely reduce sulfation of the heparan sulfate chains (Fig. 4 e).

The potentiation of growth factor action by heparan sulfate proteoglycans is thought to depend on formation of ternary complexes in which the heparan sulfate chain acts as a scaffold to approximate ligand and receptor, thus affecting signaling intensity and duration (Forsten-Williams et al., 2005). In the extracellular matrix, heparan sulfate proteoglycans also act as reservoir for growth factors (Vlodavsky et al., 1990), providing stability and enhancing the capacity for gradient formation (Lander et al., 2002). Many tumors secrete heparanase, which

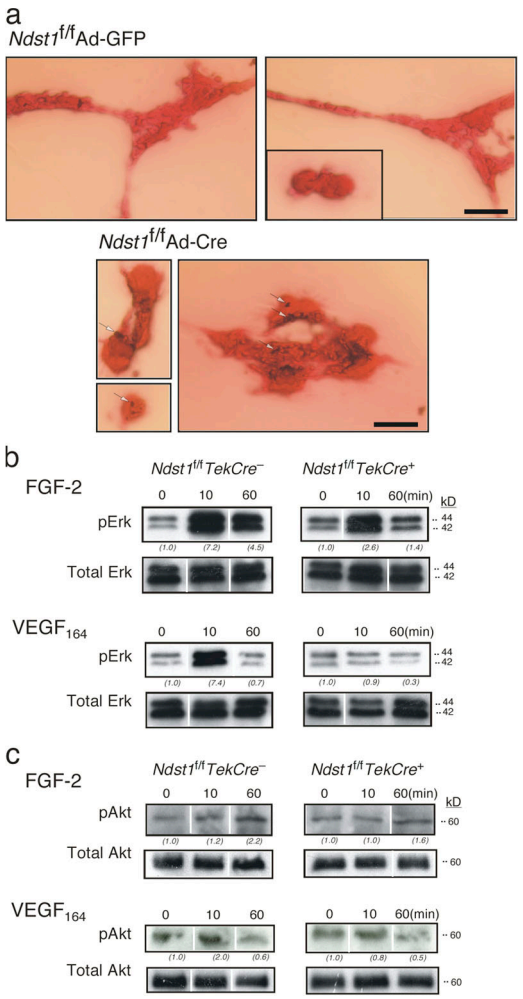

Figure 6. **Altered growth factor signaling by Ndst1-deficient microvascular endothelia.** (a) TUNEL assay was performed on mutant and wild-type endothelial cells undergoing sprouting on Matrigel. In these experiments, cells derived from *Ndst1*$^{f/f}$*Tek*Cre^{-} mice were infected with Ad-Cre (*Ndst1*$^{f/f}$ Ad-Cre) or Ad-GFP virus as a control (*Ndst1*$^{f/f}$ Ad-GFP). After infection with Ad-Cre, numerous apoptotic bodies were observed within the cell clusters (bottom, arrows). Ad-GFP–infected cells formed extensive sprouting networks that were relatively free of apoptotic bodies, and the few nonsprouting clusters that were present also were devoid of apoptotic bodies (top right, inset). Bars, 100 μm. (b) Phosphorylation of Erk (p44/p42) in response to the growth factors FGF-2 or $VEGF_{164}$ was measured by Western blotting. The bands were scanned, the intensity of the phosphorylated protein was normalized to the intensity of the nonphosphorylated protein, and the ratio was scaled to the value obtained at t = 0 (values in parentheses). Total Erk was similar in mutant and wild-type cells. No significant variation in signal intensity >60 min was observed in the absence of growth factor in mutant and wild-type endothelia. (c) Phosphorylation of Akt was measured in wild-type and mutant cells.

can degrade the extracellular matrix and liberate bound growth factors (Elkin et al., 2001; Vlodavsky et al., 2002), and overexpression of heparanase in tumor cells results in enhanced angiogenesis and tumor growth (Zcharia et al., 2004). Because endothelial cells produce matrix proteoglycans, loss of Ndst1 activity could, in theory, result in reduced storage of growth factors in the surrounding matrix. Thus, reduced tumor growth in *Ndst1*$^{f/f}$*TekCre*$^{+}$ mice could reflect a combination of cell-autonomous growth factor signaling defects as well as reduced availability of growth factors in the matrix.

Heparan sulfate chains do not exist as free polysaccharides but, rather, occur covalently bound to proteoglycan core proteins. The major heparan sulfate proteoglycans in endothelial cells consist of the glycosylphosphatidylinositol-linked glypicans, membrane-spanning syndecans, and secreted proteoglycans (perlecan, agrin, and collagen XVIII). Some of these have roles in angiogenesis based on mutational studies. Mutants defective in syndecan-1 show an increase in vessel length during corneal angiogenesis, possibly because of differences in release of inflammatory mediators (Gotte et al., 2002), whereas overexpression of syndecan-1 causes abnormal angiogenesis during cutaneous wound repair (Elenius et al., 2004). In contrast, syndecan-4 deficiency impairs fetal vessels in the placental labyrinth (Ishiguro et al., 2000) and angiogenesis during wound repair (Echtermeyer et al., 2001). Deletion of exon 3 of perlecan core protein, which bears a major heparan sulfate containing domain, impairs wound angiogenesis as well as tumor angiogenesis (Zhou et al., 2004). Mice lacking collagen XVIII show delayed regression of blood vessels postnatally in the vitreous along the surface of the retina and abnormal outgrowth of retinal vessels (Fukai et al., 2002) but enhanced intimal neovascularization in atherosclerotic aortas (Moulton et al., 2004). The variation in phenotype in mutants and tissues may reflect differences in the expression of individual proteoglycans in diverse vascular beds, other functional domains within the core proteins (O'Reilly et al., 1997; Bix and Iozzo, 2005), or changes in heparan sulfate in the supporting tissue in systemic mutants rather than cell-autonomous effects on endothelial cells. Additional studies are needed to analyze the effect of altering specific proteoglycans selectively in endothelial cells.

Our findings validate heparan sulfate and the enzymes involved in its biosynthesis as potential targets for chemotherapeutic intervention. Targeting heparan sulfate could prove advantageous over strategies that focus on individual proangiogenic growth factors, such as VEGF (e.g., bevacizumab; Bergsland, 2004), as heparan sulfate can modulate the activity of multiple angiogenic factors (e.g., hepatocyte growth factor, PDGF, heparin-binding EGF, angiopoietin, tumor necrosis factor-α, interleukin-8, and others; Blackhall et al., 2001; Jiang and Couchman, 2003), most of which bind to heparan sulfate. Previous studies have shown that tumor cell proliferation also depends on heparan sulfate (for review see Fuster and Esko, 2005). Because heparan sulfate biosynthesis in endothelial cells and tumor cells utilizes a common set of enzymes, agents that target heparan sulfate would provide a two-prong approach for blocking both tumor cell division and formation of the supporting vasculature.

Materials and methods

Cell lines and cell culture

LLC LL/2 (CRL-1642; American Type Culture Collection) was grown in DME (Invitrogen) containing 1.5 g/l sodium bicarbonate and supplemented with 10% FBS (HyClone). B16BL6 murine melanoma cell line was a gift from I. Fidler (University of Texas MD Anderson Cancer Center, Houston, TX) and was grown in MEM (Invitrogen) and supplemented with 7% FBS. Murine lung microvascular endothelial cells were isolated from mice essentially as described previously (Marelli-Berg et al., 2000), except after straining, cells were mixed with 4.8 ml 17% Nycodenz

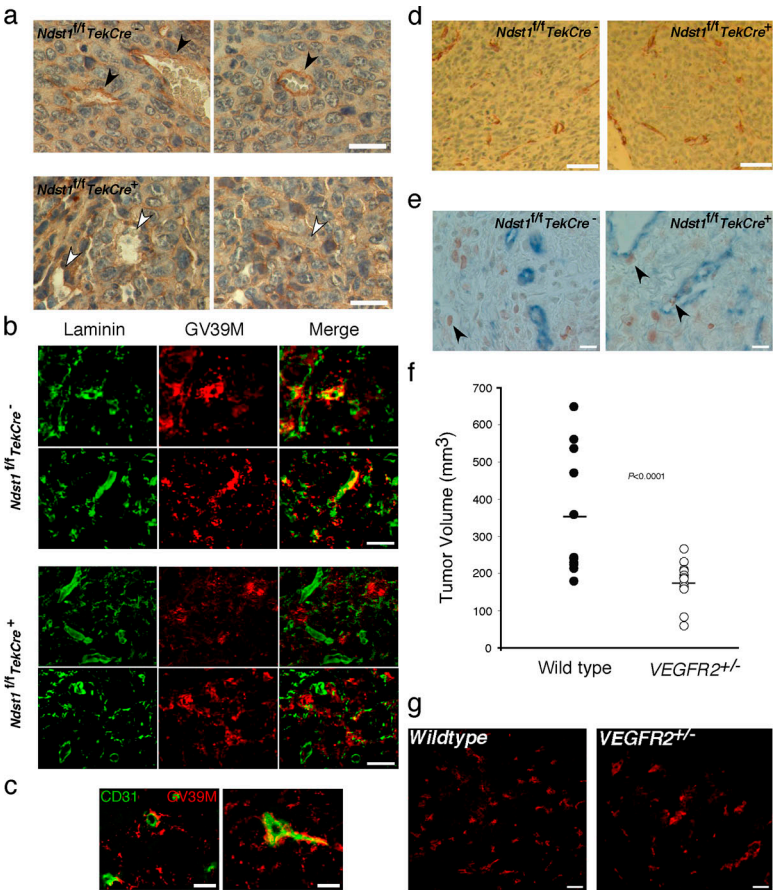

Figure 7. **Altered growth factor binding to tumor microvasculature in *Ndst1*$^{f/f}$*TekCre*$^{+}$ mice.** (a) Binding of biotinylated FGF-2 to histologic sections of LLC tumors. Solid arrowheads in wild-type sections (top) indicate strong binding in perivascular locations (surrounding birefringent red blood cells within vessels) compared with sections from mutant mice (bottom, open arrowheads). (b) Binding of GV39M to VEGF–VEGFR2 complexes and laminin mAb to vessels in tumor sections. In wild-type mice (top), GV39M (red fluorescence) colocalized with vessel-associated laminin (green), as demonstrated in merged images (yellow). Sections from mutant mice (bottom) did not show vascular colocalization of complexes with laminin. (c) Tumor sections from wild-type mice costained with CD31 mAb and GV39M (red) showed that the VEGF–VEGFR complexes were located ablumenal to CD31 staining (green). (d) Tumor sections from wild-type and mutant mice were stained for smooth muscle actin (brown) to assess the degree of vascular investment by pericytes. Mean density of stained processes among tumors in wild-type versus mutant backgrounds was comparable (n = 5 mice per group; P = 0.3). (e) Vascular endothelium-associated apoptosis in tumors was examined by labeling for CD31 (blue) and TUNEL (brown). Vasculature in tumors from mutant mice showed occasional vessel-associated apoptotic bodies (right, arrowheads), whereas any TUNEL reaction in wild-type sections was only associated tumor nuclei (left, arrowhead). (f) Growth of tumors on a *VEGFR2* heterozygous background. LLC tumors were grown on the hindquarters of wild type as well as *VEGFR2*$^{+/-}$ mice. Tumor volumes at 15 d are shown as scatter plots for wild type (n = 11 mice; solid circles) and *VEGFR2* heterozygous mutants (n = 12 mice; open circles), with mean values indicated by horizontal bars on the graph. (g) Tumor microvasculature stained by anti-CD31 mAb (red) in *VEGFR2* mutant sections was also altered (right) relative to wild type (left). Bars: (a, d, and g) 50 μm; (b) 15 μm; (c and e) 20 μm.

(Sigma-Aldrich) in Gey's balanced salt solution, overlaid with 1 ml PBS (Dulbecco and Vogt, 1954), and centrifuged at 1,400 *g*, and the endothelial rich band was collected. Cells were then labeled with rat anti–mouse CD31 (0.2 μg/10^6 cells; Caltag), incubated with goat anti–rat antibody conjugated to magnetic beads, and passed over a magnetic column (Miltenyi Biotec) followed by washing, and purified endothelia were eluted from the column into gelatin-coated plates. Cells were maintained one or two passages in DME supplemented with 20% FBS, 100 μg/ml endothelial growth supplement (Sigma-Aldrich), 100 μg/ml heparin (Scientific Protein Laboratories), and nonessential amino acids (Invitrogen). Culture media were supplemented with 100 U/ml penicillin and 100 μg/ml streptomycin. All cells were maintained under an atmosphere of 5% CO_2 and 100% humidity at 37°C. Cell proliferation was examined using the Cell Titer-Blue viability assay (Promega) on primary endothelia. Cells were plated at 5,000 cells/well in 96-well plates, grown in complete medium, and assayed on successive days for fluorescence (excitation 488 nm/emission 575 nm; CytoFluor II fluorimeter) after addition of Cell Titer-Blue reagent according to the manufacturer's instructions. Fluorescence is proportional to the number of viable cells.

Animals

C57Bl/6 mice harboring a conditional mutation in exon 2 of *Ndst1* (*Ndst1*$^{f/f}$) were crossed with transgenic mice expressing Cre recombinase under control of the *Tek* (Tie2 receptor) promoter/enhancer (*TekCre*$^{+}$; Kisanuki et al., 2001; Wang et al., 2005). *Ndst1*$^{f/f}$ *TekCre*$^{+}$ males were mated with *Ndst1*$^{f/f}$ *TekCre*$^{-}$ females generating equal numbers of mutant and wild-type animals. Genotyping of mice was performed by PCR using genomic DNA from tail biopsies as described previously (Wang et al., 2005). Mice heterozygous for VEGFR-2 (*VEGFR-2*$^{+/-}$) were purchased from The Jackson Laboratory, with genotyping performed using primers as described previously (Shalaby et al., 1995). All animals were fully backcrossed on C57Bl/6 background (>10 generations). Mice were housed under barrier conditions in AAALAC-approved vivaria, following standards and procedures approved by the local Institutional Animal Care and Use Committee. They were weaned at 3 wk, maintained on a 12-h light–dark cycle, and fed water and standard rodent chow *ad libitum*.

Quantitative PCR

To assess the efficiency of *Ndst1* inactivation, quantitative real-time PCR (Applied Biosystems) on genomic DNA was performed using primers flanking the downstream loxP recombination site of the *Ndst1* floxed construct (Grobe et al., 2005; n = 3 per group). Cycle threshold values from duplicate assays were used to determine the initial starting quantity of loxP DNA from mutant versus wild-type genomic DNA samples.

To examine endothelial *Ndst1-4* mRNA, total RNA was isolated from mutant versus wild-type primary lung endothelia, reverse transcribed (Superscript III; Invitrogen), and amplified using gene-specific intron-spanning primers (primer sequences: *Ndst1* forward, GGACATCTGGTCTAAG, and reverse, GATGCCTTTGTGATAG; *Ndst2* forward, TGGTCCAAGGAGAAAACCTG, and reverse, GGTACGACCTCCGAGTCAAA; *Ndst3* forward, CCACTGCCTTGTGTC, and reverse, GGAGTACGCTCGGTC; *Ndst4* forward, CTAACTACTTCCACTC, and reverse, ATGTGCACTGCATACC). Cycle threshold values from triplicate assays were used to calculate fold expression compared with expression of β-actin in the same sample.

Tumor growth studies

Tumor cells were harvested with Trypsin/EDTA (Invitrogen) and were inoculated subcutaneously at 4 × 10^5 cells per mouse in 50 μl DME into the left hindquarters of 10–12 wk-old mice. Tumor growth was measured using calipers over a 15-d period, and tumor volume was estimated using the following formula: vol = length × (width)^2/2. Mice were killed after 15 d (beyond which tumor ulceration became frequent), and their tumors were dissected, measured directly with calipers, and removed for cryo- and formalin fixation for further histologic analysis. Mouse bone marrow transplantation studies were performed as previously described (Wang et al., 2005). In a pilot experiment, all nontransplanted irradiated mice died within 1 wk. Conversely, all mice that underwent marrow transplantation survived until termination of the tumor experiment without ill appearance.

Immunohistochemical analysis of tumor microvasculature

Formalin-fixed and deparaffinized embedded sections from 15-d subcutaneous tumors were stained with hematoxylin/eosin. Labeling of tumor vasculature was performed using rat anti–mouse CD31 (1:200; BD Biosciences)

and biotinylated goat anti–rat secondary antibody (1:100; BD Biosciences) and detected using HRP-conjugated streptavidin (1:500; Jackson ImmunoResearch Laboratories). Development with AEC chromogen (Vector Laboratories) was followed by counterstaining with Mayer's hematoxylin. Microvascular density on tumor sections was quantified by examining the number of vessels per 400× microscopic field over five fields per section. Fluorescence staining was performed using biotinylated secondary antibodies and treatment with Cy3-conjugated streptavidin (1:500; Jackson ImmunoResearch Laboratories) on frozen tumor sections. In a separate experiment, sections were incubated with rabbit anti-vWF antibody (DakoCytomation), and bound antibodies were detected using HRP-conjugated anti–rabbit antibody (1:100; Jackson ImmunoResearch Laboratories) followed by AEC chromogen/Mayer's counterstain. Microvasculature was quantified by a pathologist blinded to slide identification. Staining of tumor leukocytes and smooth muscle actin was accomplished on paraffin-embedded sections exposed to biotin-conjugated rat anti–mouse CD45 antibody (1:200; BD Biosciences) or rabbit anti–mouse SmA antibody (1:50; NeoMarkers), respectively, with secondary antibodies, development, and counterstaining as described above. Density of SmA-positive processes was quantified for each tumor section by calculating the mean number of stained vessels per 400× field among six fields per section. Fluorescence-stained tumor microvasculature was examined in cryopreserved tumor specimens by acetone fixation of frozen sections, exposure to anti-CD31 mAb, biotinylated secondary antibodies, and treatment with Cy3-conjugated streptavidin (1:500; Jackson ImmunoResearch Laboratories). Vascular endothelial apoptosis in tumor sections was measured on acetone-fixed frozen sections treated with anti-CD31 mAb, biotinylated secondary antibodies, and AP-conjugated streptavidin followed by development with Vector Blue AP Substrate kit (Vector Laboratories) according to the manufacturer's instructions. Colabeling with TUNEL was performed on the same sections (In Situ Cell Death Detection kit; Roche) and developed using AEC chromogen (Vector Laboratories) according to the manufacturer's instructions.

In situ microvascular FGF-2 reactivity was assessed on frozen tissue sections by incubating specimens with biotinylated FGF-2 (Bai et al., 1999), and bound factor was detected with HRP-conjugated streptavidin (1:500; Jackson ImmunoResearch Laboratories). For detection of VEGF–VEGFR2 complexes, acetone-fixed frozen sections were labeled with biotinylated GV39M antibody (1:50; East Coast Biologics) followed by treatment with Cy3-conjugated streptavidin (1:500; Jackson ImmunoResearch Laboratories). Laminin in the same sections was visualized by treatment with rabbit anti-laminin antibody (1:500; DakoCytomation) followed by FITC-labeled goat anti–rabbit antibody (1:50; Chemicon).

All microscopy for immunohistology was performed using a microscope (Axiolab; Carl Zeiss MicroImaging, Inc.) with 20× (Plan-Neofluar/0.5), 40× (Achroplan/0.65), or 100× oil (Plan-Neofluar/1.30) objectives, with all image acquisition taken at room temperature. A 3CCD camera (DKC 5000; Sony) was used for digital image acquisition and captured using NIH ImageJ (Scion Image v. 1.60) software. Image processing and storage (TIFF format) was performed using Photoshop software (Adobe). All fluorescence images were captured using epifluorescence (source for excitation was FluoArc [Carl Zeiss MicroImaging, Inc.]) with appropriate barrier filters on the same microscope system and using fluorochromes applied to tissues/cells as described.

Intravital studies of tumor angiogenesis

LLC LL/2 cells were resuspended in 10 ml complete medium at (2×10^6 cells/ml) and were rocked in a 50-ml silicon-coated flask on a gyratory shaker in culture. After 48–72 h, tumor spheroids of similar diameters (600–1,000 μm) were selected, washed in serum-free medium, and individually placed into dorsal skinfold chambers using a sterile plastic pipette as previously described (Borgstrom et al., 1996). Observations of tumor angiogenesis were made day 12 after tumor spheroid implantation in mutant and wild-type mice as described previously (Manegold et al., 2003). Unanesthetized mice were placed in a plexiglass tube containing a longitudinal slit from which the chamber projected for exposure to the microscope. The tube was immobilized on a plexiglass platform, which was placed on the stage of an intravital microscope (Biomed; Leitz) for viewing the tumor spheroid microcirculation. Images for all mice were recorded at room temperature through a silicone intensified tube camera (SIT68; DAGE-MTI) attached to the microscope (Nikon) using 4× or 10× water-immersion objectives. The camera was connected to a monitor (Panasonic) and an S-VHS video recorder (HC-6600; JVC). For each chamber, the tumor spheroid vasculature was identified using a 4× objective, and regions of highest tumor vascular density were recorded with the 10× objective. Still images of four to six tumor spheroid fields per chamber were recorded at 100× magnification and scanned for grid intersection using a 12 × 12 grid overlay that overlies the image, and branch points per field were measured using Photoshop CS2. Digitized images were also analyzed on Volocity 2.6.1 software (Improvision), which was used to obtain total linear (skeletal) length of vasculature per field, as well as mean vascular caliber per field.

Mouse wound induction and contraction

Under general anesthesia, mice were wounded using a 3-mm-diameter full-thickness dorsal skin punch biopsy. Wounds were then photographed daily over 4 d after injury, and wound area was measured using ImageJ software. The wounds were biopsied to include the margin to normal surrounding skin and snap-frozen in Tissue-Tek OCT (Sakura), and median sections were taken to include the wound fibrin plug at center, flanked by the wound granulation tissue and surrounding normal dermis/epidermis. Acetone-fixed sections were incubated with biotinylated anti–mouse CD31 (1:100; BD Biosciences), followed by HRP-conjugated streptavidin (1:500; Jackson ImmunoResearch Laboratories). Wound microvascular density for any given mouse was then determined by calculating the mean number of CD31+ processes per 400× field using four fields surrounding the wound center.

FGF-2 and $VEGF_{164}$ binding to mutant endothelial cells and heparan sulfate

Primary lung endothelial cells were harvested at the first or second passage using 5 mM EDTA in PBS. The cells were treated with heparin (1 mg/ml in PBS), washed with PBS, and incubated with biotinylated 0.6 μg/ml FGF-2 in buffer (0.5% BSA/2 mM EDTA in PBS) at 4°C for 1 h with gentle stirring on an orbital shaker (Bai et al., 1999). Bound FGF-2 was detected by flow cytometry using streptavidin-phycoerythrin. A set of cells was exposed only to streptavidin-phycoerythrin as a negative control. To detect VEGF binding, cells (4×10^6/ml) were incubated for 1 h at 4°C with recombinant human biotinylated $VEGF_{165}$ (1.1 μg/ml in PBS; R&D Systems). Bound $VEGF_{165}$ was detected with avidin-FITC reagent (1:1,000; R&D Systems) and flow cytometry. As controls, some cells were incubated with an irrelevant biotinylated protein (soybean trypsin inhibitor) or Alexa Fluor 488–conjugated EGF (Invitrogen; each at 8 μg/ml for 45 min at 4°C) followed by flow cytometry.

Primary lung endothelia were labeled for 48 h with 37 μCi/ml $H_2{}^{35}SO_4$ (655 Ci/mmol; NEN Life Science Products) in reduced-sulfate medium (Ham's F12 containing 10% dialyzed, filter-sterilized FBS). Isolation of purified heparan [^{35}S]sulfate from cultured cells was performed essentially as described previously (Bame and Esko, 1989). Binding of 0.2 μg FGF-2 and 1 μg $VEGF_{164}$ was measured using a nitrocellulose filter binding assay using 5,000 cpm per assay (Kreuger et al., 2003). Controls included competition with 100 μg/ml heparin or use of bovine serum albumin in place of growth factor.

[^{3}H]Heparan sulfate was prepared from primary endothelial cells by culturing them in growth medium containing [6-^{3}H]glucosamine and 1 mM reduced glucose. Radiolabeled chains were degraded with heparinases and analyzed by anion-exchange HPLC as described previously (Toyoda et al., 1997).

Angiogenesis assays on reconstituted extracellular matrix

Murine lung endothelial cells were isolated from 8–12-wk-old mutant mice or their wild-type littermates as described previously (Wang et al., 2005). Purity was assessed by flow cytometry using CD31 mAb (FACSCalibur; BD Biosciences), uptake of DiI-acetylated-LDL (10 μg/ml; Biomedical Technologies), and reaction with polyclonal antibody to von Willebrand factor (DakoCytomation).

Matrigel (BD Biosciences) was added to each well of a 96-well plate and allowed to polymerize at 37°C for 1 h. Mutant or wild-type cells at first or second passage were harvested with trypsin/EDTA (BioWhittaker) and resuspended in DME/20% FBS. Cells (5,000/well) were then added to duplicate wells in 100 μl of growth medium in the presence or absence of recombinant FGF-2 (Invitrogen) or murine $VEGF_{164}$ (Calbiochem). In a separate experiment, additional wells were seeded in the presence or absence of heparinase at 0.3 mU/ml (heparin lyase III; Seikagaku) and 10 ng/ml FGF-2. After 48 h, the degree of endothelial sprouting over the gel surface was measured by determining the net lengths of endothelial processes (in duplicate wells) viewed under phase-contrast light microscopy. The data is reported as fold stimulation relative to baseline growth without added growth factor. In some experiments, 100 μg/ml of unfractionated heparin (Scientific Protein Laboratories) was added to the wells during the sprouting period.

SDS-PAGE and Western blotting

Primary lung endothelial cells were seeded at equal density on gelatin-coated 12-well culture dishes immediately after harvest from the animals and allowed to grow to near confluence under standard culture conditions.

After incubation for 4 h in serum-free DME without supplements, cells were exposed to FGF-2 or $VEGF_{164}$ (10 ng/ml) for 10–60 min. Samples were solubilized and mixed with an equal volume of 125 mM Tris-HCl, pH 6.8, 4% SDS, 20% glycerol, 100 mM dithiothreitol, and 0.02% bromophenol blue. They were separated by electrophoresis in 4–15% gradient gels followed by electrotransfer to a nitrocellulose membrane, which was then probed using a polyclonal antibody (1:1,000; Cell Signaling Technology) that detects phosphorylated Thr^{202}/Tyr^{204} forms of p44/42 MAPKs (Erk1/2). Bound antibody was detected using peroxidase-conjugated anti–rabbit antibody (1:2,000; Bio-Rad Laboratories) followed by visualization using SuperSignal chemiluminescent substrate for HRP detection (Pierce Chemical Co.). To ensure equal protein loading, membranes were stripped and reprobed using polyclonal antibodies against total Erk1/2. In a separate experiment, a subset of wells was treated with 0.5 mU/ml heparinase during the periods of serum starvation and growth factor stimulation. For Akt signaling, membranes were probed using 1:1,000 anti-phospho (Ser^{473})-Akt monoclonal antibody (Cell Signaling Technology). The bands were quantified by measurement of band intensity relative to background on a densitometer (GS800; Bio-Rad Laboratories).

Apoptosis assay on reconstituted extracellular matrix

Mutant cells were generated by transfection of subconfluent *Ndst1*$^{f/f}$*Tek*Cre^{-} primary murine lung endothelia with Adenoviral-Cre (Ad-Cre; UCSD Gene Therapy Core) at 10^9 pfu/ml for 1.5 h in normal culture growth medium. Infection with Adenoviral-GFP (Ad-GFP) was used as a control. Cells were added to Matrigel-coated wells in chamber slides. Permeabilization and TUNEL labeling were performed directly on chamber slides according to the manufacturer's instructions (In Situ Cell Death Detection kit; Roche), and samples were stained with Vector Blue Alkaline Phosphatase Substrate kit (Vector Laboratories) and nuclear fast red stain.

Statistics

Mean values of tumor volume, microvascular density on tumor sections or wound sections, microvascular skeletal length, caliber, grid intersection, and branching, and mean relative sprouting responses on extracellular matrix, were compared using one-tailed *t* tests. $P < 0.05$ was considered significant. Comparison of wound contraction rates in mutant versus wild-type mice was performed using a two-factor repeated-measures analysis of variance, testing for group differences in the change over time (SPSS Software v. 13.0).

We thank N. Varki and L. Gapuz for assistance with immunohistology, P. Clopton for assistance with statistical analysis, and R. Brekken and R.S. Johnson for advice with VEGF immunodetection methods and valuable discussions (University of California, San Diego). We also thank S. Rought of the UCSD Center for AIDS Research Genomics Core Laboratory for assistance with quantitative PCR.

This work was supported by a U.S. Veteran's Administration Research Career Development Award and a Lopiccola Fellowship Award (M.M. Fuster), National Institutes of Health grants HD52920 and HL57345 (J.D. Esko), and the Infection and Wound Repair Core (supported through grants HL57345 [R.L. Gallo] and AI35796 [P. Sriramarao]).

The authors declare no competing financial interests.

Submitted: 18 October 2006
Accepted: 26 March 2007

References

Bai, X., G. Wei, A. Sinha, and J.D. Esko. 1999. Chinese hamster ovary cell mutants defective in glycosaminoglycan assembly and glucuronosyltransferase I. *J. Biol. Chem.* 274:13017–13024.

Bame, K.J., and J.D. Esko. 1989. Undersulfated heparan sulfate in a Chinese hamster ovary cell mutant defective in heparan sulfate N-sulfotransferase. *J. Biol. Chem.* 264:8059–8065.

Bergsland, E.K. 2004. Update on clinical trials targeting vascular endothelial growth factor in cancer. *Am. J. Health Syst. Pharm.* 61:S12–S20.

Bix, G., and R.V. Iozzo. 2005. Matrix revolutions: "tails" of basement-membrane components with angiostatic functions. *Trends Cell Biol.* 15:52–60.

Blackhall, F.H., C.L.R. Merry, E.J. Davies, and G.C. Jayson. 2001. Heparan sulfate proteoglycans and cancer. *Br. J. Cancer.* 85:1094–1098.

Borgstrom, P., K.J. Hillan, P. Sriramarao, and N. Ferrara. 1996. Complete inhibition of angiogenesis and growth of microtumors by anti-vascular endothelial growth factor neutralizing antibody: novel concepts of angiostatic therapy from intravital videomicroscopy. *Cancer Res.* 56:4032–4039.

Brekken, R.A., and P.E. Thorpe. 2001. VEGF-VEGF receptor complexes as markers of tumor vascular endothelium. *J. Control. Release.* 74:173–181.

Brekken, R.A., X. Huang, S.W. King, and P.E. Thorpe. 1998. Vascular endothelial growth factor as a marker of tumor endothelium. *Cancer Res.* 58:1952–1959.

Carmeliet, P., and R.K. Jain. 2000. Angiogenesis in cancer and other diseases. *Nature.* 407:249–257.

Constien, R., A. Forde, B. Liliensiek, H.J. Grone, P. Nawroth, G. Hammerling, and B. Arnold. 2001. Characterization of a novel EGFP reporter mouse to monitor Cre recombination as demonstrated by a Tie2 Cre mouse line. *Genesis.* 30:36–44.

Dulbecco, R., and M. Vogt. 1954. Plaque formation and isolation of pure cell lines with poliomyelitis viruses. *J. Exp. Med.* 99:167–182.

Echtermeyer, F., M. Streit, S. Wilcox-Adelman, S. Saoncella, F. Denhez, M. Detmar, and P. Goetinck. 2001. Delayed wound repair and impaired angiogenesis in mice lacking syndecan-4. *J. Clin. Invest.* 107: R9–R14.

Elenius, V., M. Gotte, O. Reizes, K. Elenius, and M. Bernfield. 2004. Inhibition by the soluble syndecan-1 ectodomains delays wound repair in mice overexpressing syndecan-1. *J. Biol. Chem.* 279:41928–41935.

Elkin, M., N. Ilan, R. Ishai-Michaeli, Y. Friedmann, O. Papo, I. Pecker, and I. Vlodavsky. 2001. Heparanase as mediator of angiogenesis: mode of action. *FASEB J.* 15:NIL33–NIL48.

Ellis, L.M., and P. Kirkpatrick. 2005. Bevacizumab. *Nat. Rev. Drug Discov.* 4(Suppl.):S8–S9.

Esko, J.D., and S.B. Selleck. 2002. Order out of chaos: assembly of ligand binding sites in heparan sulfate. *Annu. Rev. Biochem.* 71:435–471.

Folkman, J. 1992. The role of angiogenesis in tumor growth. *Semin. Cancer Biol.* 3:65–71.

Forsberg, E., G. Pejler, M. Ringvall, C. Lunderius, B. Tomasini-Johansson, M. Kusche-Gullberg, I. Eriksson, J. Ledin, L. Hellman, and L. Kjellén. 1999. Abnormal mast cells in mice deficient in a heparin-synthesizing enzyme. *Nature.* 400:773–776.

Forsten-Williams, K., C.C. Chua, and M.A. Nugent. 2005. The kinetics of FGF-2 binding to heparan sulfate proteoglycans and MAP kinase signaling. *J. Theor. Biol.* 233:483–499.

Fukai, N., L. Eklund, A.G. Marneros, S.P. Oh, D.R. Keene, L. Tamarkin, M. Niemela, M. Ilves, E. Li, T. Pihlajaniemi, and B.R. Olsen. 2002. Lack of collagen XVIII/endostatin results in eye abnormalities. *EMBO J.* 21:1535–1544.

Fuster, M.M., and J.D. Esko. 2005. The sweet and sour of cancer: glycans as novel therapeutic targets. *Nat. Rev. Cancer.* 5:526–542.

Gotte, M., A.M. Joussen, C. Klein, P. Andre, D.D. Wagner, M.T. Hinkes, B. Kirchhof, A.P. Adamis, and M. Bernfield. 2002. Role of syndecan-1 in leukocyte-endothelial interactions in the ocular vasculature. *Invest. Ophthalmol. Vis. Sci.* 43:1135–1141.

Grobe, K., M. Inatani, S.R. Pallerla, J. Castagnola, Y. Yamaguchi, and J.D. Esko. 2005. Cerebral hypoplasia and craniofacial defects in mice lacking heparan sulfate Ndst1 gene function. *Development.* 132:3777–3786.

Grunstein, J., J.J. Masbad, R. Hickey, F. Giordano, and R.S. Johnson. 2000. Isoforms of vascular endothelial growth factor act in a coordinate fashion to recruit and expand tumor vasculature. *Mol. Cell. Biol.* 20:7282–7291.

Holmborn, K., J. Ledin, E. Smeds, I. Eriksson, M. Kusche-Gullberg, and L. Kjellen. 2004. Heparan sulfate synthesized by mouse embryonic stem cells deficient in NDST1 and NDST2 is 6-O-sulfated but contains no N-sulfate groups. *J. Biol. Chem.* 279:42355–42358.

Holmgren, L., M.S. O'Reilly, and J. Folkman. 1995. Dormancy of micrometastases: balanced proliferation and apoptosis in the presence of angiogenesis suppression. *Nat. Med.* 1:149–153.

Humphries, D.E., G.W. Wong, D.S. Friend, M.F. Gurish, W.T. Qiu, C.F. Huang, A.H. Sharpe, and R.L. Stevens. 1999. Heparin is essential for the storage of specific granule proteases in mast cells. *Nature.* 400:769–772.

Iozzo, R.V. 2005. Basement membrane proteoglycans: from cellar to ceiling. *Nat. Rev. Mol. Cell Biol.* 6:646–656.

Iozzo, R.V., and J.D. San Antonio. 2001. Heparan sulfate proteoglycans: heavy hitters in the angiogenesis arena. *J. Clin. Invest.* 108:349–355.

Ishiguro, K., K. Kadomatsu, T. Kojima, H. Muramatsu, E. Nakamura, M. Ito, T. Nagasaka, H. Kobayashi, K. Kusugami, H. Saito, and T. Muramatsu. 2000. Syndecan-4 deficiency impairs the fetal vessels in the placental labyrinth. *Dev. Dyn.* 219:539–544.

Izvolsky, K.I., L. Zhong, L. Wei, Q. Yu, M.A. Nugent, and W.V. Cardoso. 2003. Heparan sulfates expressed in the distal lung are required for Fgf10 binding to the epithelium and for airway branching. *Am. J. Physiol. Lung Cell. Mol. Physiol.* 285:L838–L846.

Jain, R.K. 2003. Molecular regulation of vessel maturation. *Nat. Med.* 9:685–693.

Jain, R.K. 2005. Normalization of tumor vasculature: an emerging concept in antiangiogenic therapy. *Science.* 307:58–62.

Jakobsson, L., J. Kreuger, K. Holmborn, L. Lundin, I. Eriksson, L. Kjellen, and L. Claesson-Welsh. 2006. Heparan sulfate in trans potentiates VEGFR-mediated angiogenesis. *Dev. Cell.* 10:625–634.

Jiang, X., and J.R. Couchman. 2003. Perlecan and tumor angiogenesis. *J. Histochem. Cytochem.* 51:1393–1410.

Joyce, J.A., C. Freeman, N. Meyer-Morse, C.R. Parish, and D. Hanahan. 2005. A functional heparan sulfate mimetic implicates both heparanase and heparan sulfate in tumor angiogenesis and invasion in a mouse model of multistage cancer. *Oncogene.* 24:4037–4051.

Kisanuki, Y.Y., R.E. Hammer, J. Miyazaki, S.C. Williams, J.A. Richardson, and M. Yanagisawa. 2001. Tie2-Cre transgenic mice: a new model for endothelial cell-lineage analysis *in vivo*. *Dev. Biol.* 230:230–242.

Kreuger, J., U. Lindahl, and P. Jemth. 2003. Nitrocellulose filter binding to assess binding of glycosaminoglycans to proteins. *Methods Enzymol.* 363:327–339.

Lander, A.D., Q. Nie, and F.Y. Wan. 2002. Do morphogen gradients arise by diffusion? *Dev. Cell.* 2:785–796.

Ledin, J., M. Ringvall, M. Thuveson, I. Eriksson, M. Wilen, M. Kusche-Gullberg, E. Forsberg, and L. Kjellen. 2006. Enzymatically active N-deacetylase/N-sulfotransferase-2 is present in liver but does not contribute to heparan sulfate N-sulfation. *J. Biol. Chem.* 281:35727–35734.

Liekens, S., E. De Clercq, and J. Neyts. 2001. Angiogenesis: regulators and clinical applications. *Biochem. Pharmacol.* 61:253–270.

Lin, X., E.M. Buff, N. Perrimon, and A.M. Michelson. 1999. Heparan sulfate proteoglycans are essential for FGF receptor signaling during *Drosophila* embryonic development. *Development.* 126:3715–3723.

Lin, X., G. Wei, Z.Z. Shi, L. Dryer, J.D. Esko, D.E. Wells, and M.M. Matzuk. 2000. Disruption of gastrulation and heparan sulfate biosynthesis in EXT1-deficient mice. *Dev. Biol.* 224:299–311.

Lyden, D., K. Hattori, S. Dias, C. Costa, P. Blaikie, L. Butros, A. Chadburn, B. Heissig, W. Marks, L. Witte, et al. 2001. Impaired recruitment of bone-marrow-derived endothelial and hematopoietic precursor cells blocks tumor angiogenesis and growth. *Nat. Med.* 7:1194–1201.

Manegold, P.C., J. Hutter, S.A. Pahernik, K. Messmer, and M. Dellian. 2003. Platelet-endothelial interaction in tumor angiogenesis and microcirculation. *Blood.* 101:1970–1976.

Marelli-Berg, F.M., E. Peek, E.A. Lidington, H.J. Stauss, and R.I. Lechler. 2000. Isolation of endothelial cells from murine tissue. *J. Immunol. Methods.* 244:205–215.

Moulton, K.S., B.R. Olsen, S. Sonn, N. Fukai, D. Zurakowski, and X. Zeng. 2004. Loss of collagen XVIII enhances neovascularization and vascular permeability in atherosclerosis. *Circulation.* 110:1330–1336.

O'Reilly, M.S., T. Boehm, Y. Shing, N. Fukai, G. Vasios, W.S. Lane, E. Flynn, J.R. Birkhead, B.R. Olsen, and J. Folkman. 1997. Endostatin: an endogenous inhibitor of angiogenesis and tumor growth. *Cell.* 88:277–285.

Ono, K., H. Hattori, S. Takeshita, A. Kurita, and M. Ishihara. 1999. Structural features in heparin that interact with VEGF165 and modulate its biological activity. *Glycobiology.* 9:705–711.

Pallerla, S.R., Y. Pan, X. Zhang, J.D. Esko, and K. Grobe. 2007. Heparan sulfate Ndst1 gene function variably regulates multiple signaling pathways during mouse development. *Dev. Dyn.* 236:556–563.

Pan, Y., A. Woodbury, J.D. Esko, K. Grobe, and X. Zhang. 2006. Heparan sulfate biosynthetic gene Ndst1 is required for FGF signaling in early lens development. *Development.* 133:4933–4944.

Parsons-Wingerter, P., K.E. Elliott, J.I. Clark, and A.G. Farr. 2000. Fibroblast growth factor-2 selectively stimulates angiogenesis of small vessels in arterial tree. *Arterioscler. Thromb. Vasc. Biol.* 20:1250–1256.

Penc, S.F., B. Pomahac, T. Winkler, R.A. Dorschner, E. Eriksson, M. Herndon, and R.L. Gallo. 1998. Dermatan sulfate released after injury is a potent promoter of fibroblast growth factor-2 function. *J. Biol. Chem.* 273:28116–28121.

Presta, M., P. Dell'Era, S. Mitola, E. Moroni, R. Ronca, and M. Rusnati. 2005. Fibroblast growth factor/fibroblast growth factor receptor system in angiogenesis. *Cytokine Growth Factor Rev.* 16:159–178.

Qu-Hong, J.A. Nagy, D.R. Senger, H.F. Dvorak, and A.M. Dvorak. 1995. Ultrastructural localization of vascular permeability factor/vascular endothelial growth factor (VPF/VEGF) to the abluminal plasma membrane and vesiculovacuolar organelles of tumor microvascular endothelium. *J. Histochem. Cytochem.* 43:381–389.

Ringvall, M., J. Ledin, K. Holmborn, T. Van Kuppevelt, F. Ellin, I. Eriksson, A.M. Olofsson, L. Kjellén, and E. Forsberg. 2000. Defective heparan sulfate biosynthesis and neonatal lethality in mice lacking N-deacetylase/N-sulfotransferase-1. *J. Biol. Chem.* 275:25926–25930.

Ruhrberg, C. 2003. Growing and shaping the vascular tree: multiple roles for VEGF. *Bioessays.* 25:1052–1060.

Shalaby, F., J. Rossant, T.P. Yamaguchi, M. Gertsenstein, X.F. Wu, M.L. Breitman, and A.C. Schuh. 1995. Failure of blood-island formation and vasculogenesis in Flk-1-deficient mice. *Nature.* 376:62–66.

Shinde Patil, V.R., E.B. Friedrich, A.E. Wolley, R.E. Gerszten, J.R. Allport, and R. Weissleder. 2005. Bone marrow-derived $lin^{-}c\text{-}kit^{+}Sca\text{-}1^{+}$ stem cells do not contribute to vasculogenesis in Lewis lung carcinoma. *Neoplasia.* 7:234–240.

Stickens, D., B.M. Zak, N. Rougier, J.D. Esko, and Z. Werb. 2005. Mice deficient in Ext2 lack heparan sulfate and develop exostoses. *Development.* 132:5055–5068.

Taylor, K.R., J.A. Rudisill, and R.L. Gallo. 2005. Structural and sequence motifs in dermatan sulfate for promoting fibroblast growth factor-2 (FGF-2) and FGF-7 activity. *J. Biol. Chem.* 280:5300–5306.

Toyoda, H., T. Nagashima, R. Hirata, T. Toida, and T. Imanari. 1997. Sensitive high-performance liquid chromatographic method with detection for the determination of heparin and heparan sulfate in biological samples: application to human urinary heparan sulfate. *J. Chromatogr. B Biomed. Sci. Appl.* 704:19–24.

Turnbull, J.E., D.G. Fernig, Y. Ke, M.C. Wilkinson, and J.T. Gallagher. 1992. Identification of the basic fibroblast growth factor binding sequence in fibroblast heparan sulfate. *J. Biol. Chem.* 267:10337–10341.

Vlodavsky, I., G. Korner, R. Ishai-Michaeli, P. Bashkin, R. Bar-Shavit, and Z. Fuks. 1990. Extracellular matrix-resident growth factors and enzymes: possible involvement in tumor metastasis and angiogenesis. *Cancer Metastasis Rev.* 9:203–226.

Vlodavsky, I., O. Goldshmidt, E. Zcharia, R. Atzmon, Z. Rangini-Guatta, M. Elkin, T. Peretz, and Y. Friedmann. 2002. Mammalian heparanase: involvement in cancer metastasis, angiogenesis and normal development. *Semin. Cancer Biol.* 12:121–129.

Wang, L., M. Fuster, P. Sriramarao, and J.D. Esko. 2005. Endothelial heparan sulfate deficiency impairs L-selectin- and chemokine-mediated neutrophil trafficking during inflammatory responses. *Nat. Immunol.* 6:902–910.

Yayon, A., M. Klagsbrun, J.D. Esko, P. Leder, and D.M. Ornitz. 1991. Cell surface, heparin-like molecules are required for binding of basic fibroblast growth factor to its high affinity receptor. *Cell.* 64:841–848.

Yuan, F., Y. Chen, M. Dellian, N. Safabakhsh, N. Ferrara, and R.K. Jain. 1996. Time-dependent vascular regression and permeability changes in established human tumor xenografts induced by an anti-vascular endothelial growth factor/vascular permeability factor antibody. *Proc. Natl. Acad. Sci. USA.* 93:14765–14770.

Zcharia, E., S. Metzger, T. Chajek-Shaul, H. Aingorn, M. Elkin, Y. Friedmann, T. Weinstein, J.P. Li, U. Lindahl, and I. Vlodavsky. 2004. Transgenic expression of mammalian heparanase uncovers physiological functions of heparan sulfate in tissue morphogenesis, vascularization, and feeding behavior. *FASEB J.* 18:252–263.

Zhou, Z., J. Wang, R. Cao, H. Morita, R. Soininen, K.M. Chan, B. Liu, Y. Cao, and K. Tryggvason. 2004. Impaired angiogenesis, delayed wound healing and retarded tumor growth in perlecan heparan sulfate-deficient mice. *Cancer Res.* 64:4699–4702.